THE JOURNAL OF BIOLOGICAL CHEMISTRY VOL. 288, NO. 50, pp. 35793–35800, December 13, 2013

Insights into Distinct Modulation of α7 and α7β2 Nicotinic Acetylcholine Receptors by the Volatile Anesthetic Isoflurane*[S]

Received for publication, August 6, 2013, and in revised form, October 16, 2013 Published, JBC Papers in Press, November 5, 2013, DOI 10.1074/jbc.M113.508333

David D. Mowrey[‡§], Qiang Liu[¶], Vasyl Bondarenko[‡], Qiang Chen[‡], Edom Seyoum[‡], Yan Xu[‡‖], Jie Wu[¶], and Pei Tang[‡§**1]**

*From the Departments of [‡]Anesthesiology, [‖]Structural Biology, [§]Computational and Systems Biology, and **Pharmacology & Chemical Biology, University of Pittsburgh School of Medicine, Pittsburgh, Pennsylvania 15260 and the [¶]Division of Neurology, Barrow Neurological Institute, St. Joseph's Hospital and Medical Center, Phoenix, Arizona 85013*

Background: What determines hypersensitivity or insensitivity of β2-containing or α7 nAChRs to volatile anesthetics remains unclear.
Results: Isoflurane binds to the EC end of the TM domain, modulates channel dynamics, and inhibits channel current in β2 not α7.
Conclusion: The dynamic and structural differences between β2 and α7 affect isoflurane binding and inhibition.
Significance: Both structure and dynamics are critical for drug action.

Nicotinic acetylcholine receptors (nAChRs) are targets of general anesthetics, but functional sensitivity to anesthetic inhibition varies dramatically among different subtypes of nAChRs. Potential causes underlying different functional responses to anesthetics remain elusive. Here we show that in contrast to the α7 nAChR, the α7β2 nAChR is highly susceptible to inhibition by the volatile anesthetic isoflurane in electrophysiology measurements. Isoflurane-binding sites in β2 and α7 were found at the extracellular and intracellular end of their respective transmembrane domains using NMR. Functional relevance of the identified β2 site was validated via point mutations and subsequent functional measurements. Consistent with their functional responses to isoflurane, β2 but not α7 showed pronounced dynamics changes, particularly for the channel gate residue Leu-249(9′). These results suggest that anesthetic binding alone is not sufficient to generate functional impact; only those sites that can modulate channel dynamics upon anesthetic binding will produce functional effects.

Neuronal nicotinic acetylcholine receptors (nAChRs)[2] are pentameric ligand-gated ion channels (pLGICs) that mediate the fast synaptic response in the central and peripheral nervous systems. They are composed of α (α2–α10) and β (β2–β4) subunits and assemble to form either homo- or hetero-pLGICs. The α7 subunit mainly forms homo-pLGICs, but it can also assemble with β2 or β3 subunits to form hetero-pLGICs (1–3). nAChRs have been implicated in general anesthesia and play roles in memory (4), nociception (5), and the autonomic response (6). Different subtypes of nAChRs show distinct sensitivities to general anesthetics (7–9), even though they share high sequence homology. For instance, the α7 nAChR is insensitive to volatile anesthetics at clinically relevant concentrations, whereas the α4β2 nAChR is hypersensitive (8, 9). The underlying cause, however, remains elusive.

High resolution structures of the full-length neuronal nAChRs, including α4β2 and α7, have not been solved. However, NMR structures for the TM domains of α4, β2, and α7 subunits have been recently determined (Protein Data Bank codes 2LLY, 2LM2, and 2MAW) (10). The 4 Å resolution cryo-electron microscopy structure of the *Torpedo marmorata* nAChR (11) reveals overall structural features of nAChRs. Each subunit has an extracellular (EC) domain containing the orthosteric ligand binding site, a transmembrane (TM) domain composed of four TM helices, of which TM2 lines the pore and contains the channel gate, and an intracellular (IC) domain. High resolution x-ray structures of bacterial homologues from *Gloebacter violaceous* (GLIC) and *Erwinia chrysanthemi* (ELIC) demonstrate the same structural scaffold (12–18).

Previously, we investigated potential causes for different sensitivities of the α4β2 and α7 nAChRs to volatile general anesthetics using molecular dynamics simulations (19–21). Although multiple anesthetic binding sites were observed in α7, α4, and β2 subunits, anesthetic binding to a site at the interface between EC and TM domains of β2 produced a profound change in protein dynamics that was likely to affect channel function. On the basis of the simulation results, we proposed that the susceptibility to anesthetic perturbation in β2, but not in α7, underlies the functional sensitivity of α4β2 and insensitivity of α7 to volatile anesthetics (19). We also predicted that

* This work was supported, in whole or in part, by National Institutes of Health Grants R01GM56257 and R01GM66358 (to P. T.) and R37GM049202 (to Y. X.).

The atomic coordinates and structure factors (code 2MAW) have been deposited in the Protein Data Bank (http://wwpdb.org/).

[S] This article contains supplemental Figs. S1 and S2.

[1] To whom correspondence should be addressed: Depts. of Anesthesiology, Computational and Systems Biology, and Pharmacology & Chemical Biology, University of Pittsburgh School of Medicine, 2049 Biomedical Science Tower 3, 3501 Fifth Ave., Pittsburgh, PA 15260. Tel.: 412-383-9798; Fax: 412-648-8998; E-mail: tangp@upmc.edu.

[2] The abbreviations used are: nAChR, nicotinic acetylcholine receptor; pLGIC, pentameric ligand-gated ion channel; EC, extracellular; TM, transmembrane; IC, intracellular; VDB, ventral diagonal band; VTA, ventral tegmental area; HSQC, heteronuclear single quantum coherence; TROSY, transverse relaxation-optimized spectroscopy.

unlike $\alpha7$, $\alpha7\beta2$ would be sensitive to volatile anesthetics because of the involvement of $\beta2$ (19).

In the present study, we revealed different functional responses of the $\alpha7\beta2$ and $\alpha7$ nAChRs, expressed in neurons and *Xenopus laevis* oocytes, to the anesthetic isoflurane. We also determined the binding sites and dynamic effects of isoflurane on both the $\alpha7$ and $\beta2$ nAChR TM domains using NMR, validated the functional relevance of the identified isoflurane site via point mutations and subsequent functional measurements, and rationalized potential causes underlying the insensitivity of the $\alpha7$ channel and the hypersensitivity of the $\alpha7\beta2$ channel to isoflurane. The study provides compelling evidence that isoflurane binds to both $\alpha7$ and $\beta2$, but at different locations. More importantly, isoflurane binding induced pronounced dynamics changes in $\beta2$, particularly for the channel gate residue Leu-249(9′). In contrast, isoflurane binding to $\alpha7$ did not generate the same dynamics changes. The study conveys a message that only those sites able to modulate protein dynamics upon anesthetic binding will produce functional effects.

EXPERIMENTAL PROCEDURES

Electrophysiology Measurements—Neuron dissociation and patch clamp whole cell current recordings were performed as reported previously (3). Briefly, several 400-μm coronal slices from postnatal Wistar rats (2–3 weeks old) containing the ventral diagonal band (VDB) or the ventral tegmental area (VTA) were cut in cold (2–4 °C) artificial cerebrospinal fluid. The slices were incubated for at least 1 h in oxygenated artificial cerebrospinal fluid at room temperature (22 ± 1 °C). Thereafter, the slices were treated with Pronase (1 mg/6 ml) at 31 °C for 30 min. The medial septum/diagonal band or VTA region was micropunched out from the slices using a well polished needle. Each punched piece was then dissociated mechanically using several fire-polished micro-Pasteur pipettes in a 35-mm culture dish filled with well oxygenated, standard external solution (150 mM NaCl, 5 mM KCl, 1 mM $MgCl_2$, 2 mM $CaCl_2$, 10 mM glucose, and 10 mM HEPES, pH 7.4, with Tris-base). The separated single cells usually adhered to the bottom of the dish within 30 min. Human $\alpha7$-nAChR was expressed heterologously in transfected SH-EP1 human epithelial cells as described in detail previously (22).

Functional measurements were performed using perforated patch whole cell recordings coupled with a two-barrel drug application system (3). After the formation of whole cell configuration, an access resistance less than 30 MΩ was acceptable for voltage-clamp recordings. The series resistance was not compensated in the experiments using dissociated neurons. The data were filtered at 2 kHz, acquired at 11 kHz, and digitized on-line (Digidata 1322 series A/D board; Axon Instruments, Foster City, CA). All experiments were done at room temperature (22 ± 1 °C). Clampex 9.2 (Axon Instruments) was used for data acquisition, and Prism 3.0 (*Prismsoft Inc.*) was used for graphics and statistical calculation. For statistical analysis of multiple groups of data, one-way or multivariate analysis of variance followed by appropriate test was applied. $p < 0.05$ was considered significant, and the data are represented as mean ± S.E.

To ascertain the different sensitivity of $\alpha7\beta2$ and $\alpha7$ to isoflurane observed in neurons, we also used *Xenopus laevis* oocytes for channel expression and functional measurements. The plasmids encoding human $\alpha7$ and $\beta2$ nAChRs for oocyte expression were gifts from Prof. Lindstrom's lab at the University of Pennsylvania and Prof. Henry Lester's lab at the California Institute of Technology, respectively. To reconcile the structural and functional data, we constructed two mutants ($\alpha7$-M22′V and $\alpha7\beta2$-V22′M) for functional measurements in oocytes. The mutations were introduced by QuikChange lightning site-directed mutagenesis kit (Agilent) and confirmed by DNA sequencing. cRNAs were synthesized for $\alpha7$ and $\alpha7$-M261V(M22′V) with the mMessage mMachine SP6 kit (Ambion) and for $\beta2$ and $\beta2$-V22′M with the mMessage mMachine T7 kit (Ambion). The cRNAs were purified with the RNeasy kit (Qiagen).

Channel functions of *Xenopus laevis* oocytes (stages 5–6) expressing native and mutant nAChRs were measured by two-electrode voltage clamp experiments. For making $\alpha7\beta2$, the RNAs of $\alpha7$ and $\beta2$ were injected to each oocyte in a 1:1 ratio with a total of 25 ng. The injected oocytes were maintained at 18 °C in a modified Barth's solution (17). After being expressed for 24–36 h, the oocyte in a 20-μl recording chamber (Automate Scientific) and the ND96 buffer (23) was clamped with an OC-725C Amplifier (Warner Instruments) to a holding potential of −60 mV, and currents elicited by acetylcholine and modulated by 50-μM isoflurane were recorded. The collected data were processed using Clampex 10 software (Molecular Devices).

NMR Experiments—NMR samples of the TM domains of the $\alpha7$ and $\beta2$ human nAChRs were prepared using the protocols as reported in detail previously (10). Each NMR sample at pH 4.7 contained 0.25–0.3 mM protein, 40–60 mM lauryldimethylamine-oxide (LDAO) detergent, 5 mM sodium acetate, 10 mM NaCl, 20 mM 2-mercaptoethanol to prevent disulfide bond formation, and 5% D_2O for deuterium lock in NMR measurements. The anesthetic isoflurane was titrated into the samples using a gas tight microsyringe. The isoflurane concentration was quantified based on ^{19}F NMR using the method reported previously (24).

All NMR spectra were acquired on a Bruker Avance 600 MHz spectrometer, which was equipped with a triple-resonance inverse detection TCI cryoprobe (Bruker Instruments, Billerica, MA). ^1H-^{15}N TROSY-HSQC spectra were acquired with 1-s relaxation delay for each sample before and after adding isoflurane. Spectral windows were typically 13 ppm (1,024 data points) in the ^1H dimension and 22 ppm (128 data points) in the ^{15}N dimension. The ^1H chemical shifts were referenced to the DSS resonance at 0 ppm, and the ^{15}N chemical shifts were indirectly referenced (25).

The collected NMR data were processed using NMRPipe 4.1 and NMRDraw 1.8 (26) and analyzed using Sparky 3.10 (27). Each processed spectrum had 4,096 × 512 data points. ^1H and ^{15}N chemical shift assignments for the $\alpha7$ and $\beta2$ TM domains in the presence of isoflurane were referenced to the previous assignments for the same proteins without drugs (10). Chemical shifts and peak intensities in the NMR spectra were measured using Sparky 3.10 (27).

Visualization of Isoflurane Binding and Calculation of Cavity Volumes and Angles between TM2 and TM4—To assist visualizing isoflurane-binding sites identified by NMR experiments, we performed docking of isoflurane to NMR structures of the $\alpha7$ and $\beta2$ TM domains. The targeted docking kept only those sites consistent with the NMR results. Docking was performed with Autodock4 (28) using a Lamarckian genetic algorithm with a grid spacing of 0.375 Å. For each intrasubunit binding site suggested by the NMR data, 250 independent anesthetic dockings were performed within a cube covering ~6,600 $Å^3$ using an initial population size of 500.

The sizes of intersubunit cavities for isoflurane binding were calculated using the POVME algorithm (29). A grid encompassing the cavity in each of the 20 NMR structures of $\alpha7$ or $\beta2$ was generated with 0.5 Å grid spacing. The algorithm provided the grid points defining the cavity, which represent a subset of the total cavity points. Using MATLAB®, we determined the frequency that each point was observed in the bundle of 20 NMR structures for $\alpha7$ or $\beta2$. Points shown from at least five structures were used for highlighting the cavity in Fig. 3. Reported cavity volumes are the means ± S.E. of the volumes calculated for the 20 NMR structures. The VMD program (30) was used for visualizing molecular structures and generating figures.

The angles between TM2 and TM4 helices near the EC end of the TM domain were calculated for each of 20 structures for $\beta2$ or $\alpha7$. Vectors were fit to backbone atoms of TM2 (residues from Lys-260 to Leu-249 in $\beta2$ and from Glu-259 to Leu-248 in $\alpha7$) and TM4 (residues from Leu-454 to Phe-443 in $\beta2$ and from Met-466 to Val-455 in $\alpha7$). Angles were calculated using the cross product of the two vectors. The values reported are the mean differences between the $\beta2$ and $\alpha7$ angles ± the pooled standard error, SE_P,

$$SE_p = S_p\sqrt{\frac{1}{n_1}+\frac{1}{n_2}} \qquad \text{(Eq. 1)}$$

where

$$S_p = \sqrt{\frac{(n_1-1)s_1^2+(n_2-1)s_2^2}{n_1+n_2-2}} \qquad \text{(Eq. 2)}$$

and where n_1 and n_2 represent the two sample sizes, and s_1 and s_2 represent the two standard deviations.

RESULTS

The α7β2 nAChR Is Much More Sensitive to Isoflurane Inhibition Than the α7 nAChR—Our previous pharmacological, cell biological, and single-cell RT-PCR studies confirmed the expression, localization, and assembly of $\alpha7\beta2$ nAChRs in VDB neurons (3). Here, we used the same dissociated VDB neurons to test functional responses of $\alpha7\beta2$ nAChRs to the volatile anesthetic isoflurane. As shown in Fig. 1, the inward currents were generated by application of 10 mM choline, an agonist for $\alpha7$-containing nAChRs, in acutely dissociated neurons from mouse VDB at a holding potential of −60 mV. The peak currents were significantly reduced by 10 μM isoflurane after 2 min of isoflurane preincubation. Isoflurane preincubation reduced the maximal choline-induced activation by 37 ± 8%. The EC_{50} and Hill coefficient had no significant changes ($p = 0.58$) in the absence (3.8 ± 0.3 mM; 1.35 ± 0.32) and presence (4.1 ± 0.5 mM; 1.23 ± 0.18) of 10 μM isoflurane, suggesting that isoflurane inhibition occurs in a noncompetitive manner (Fig. 1*a*). Isoflurane inhibition of $\alpha7\beta2$-nAChR-mediated whole cell current in acutely dissociated neurons from mouse VDB was concentration-dependent with an IC_{50} of 11.7 ± 1.6 μM (Fig. 1*b*), less than 0.1 minimum alveolar concentration in human (31, 32). We

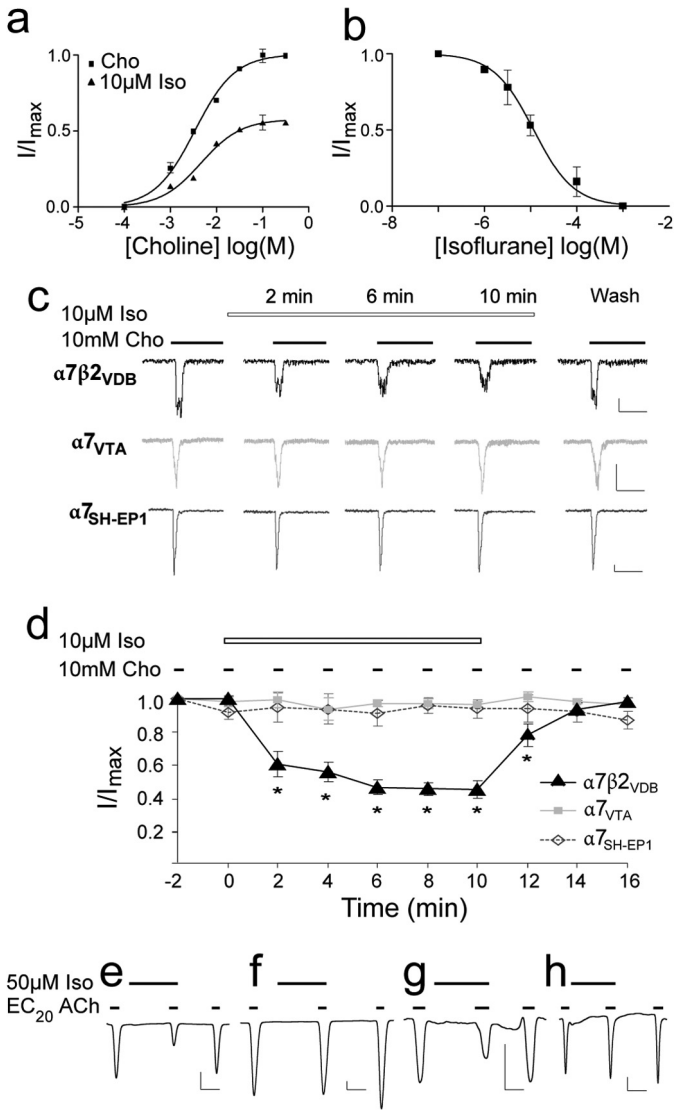

FIGURE 1. **Isoflurane inhibited function of the α7β2 but not α7 nAChRs.** *a*, the $\alpha7\beta2$ nAChRs expressed in VDB neurons were noncompetitively inhibited by 2 min of preincubation with 10 μM isoflurane (*Iso*). EC_{50} of choline (*Cho*) and Hill coefficients show no significant differences in the absence and presence of isoflurane. *b*, isoflurane inhibited $\alpha7\beta2$ with an IC_{50} of 11.7 ± 1.6 μM. Fractional currents were obtained from the mean peak currents elicited by 10 mM choline (~EC_{70}). The *error bars* are standard errors ($n = 6$). *c*, representative whole cell current traces for $\alpha7\beta2$ expressed in VDB neurons, native $\alpha7$ in VTA neurons, and heterologously human $\alpha7$ nAChRs in the SH-EP1 cells. The *vertical* and *horizontal scales* represent 50 pA and 250 ms, respectively. *d*, normalized mean (± S.E.) peak current responses of $\alpha7\beta2$ and $\alpha7$ expressed in various cells to the prolonged choline stimulation in the presence of 10 μM isoflurane ($n = 6$). Isoflurane inhibited choline-induced currents in $\alpha7\beta2$, but not in $\alpha7$. *e–h*, representative current traces for $\alpha7\beta2$ (*e*), $\alpha7$ (*f*), the $\alpha7$-M22′V mutant (*g*), and the $\alpha7\beta2$-V22′M mutant (*h*) expressed in *Xenopus* oocytes. The currents were elicited by acetylcholine at the EC_{20}, modulated by isoflurane (50 μM), and recorded by two-electrode voltage clamp at −60 mV. The *vertical* and *horizontal scales* represent 25 nA and 1 min, respectively.

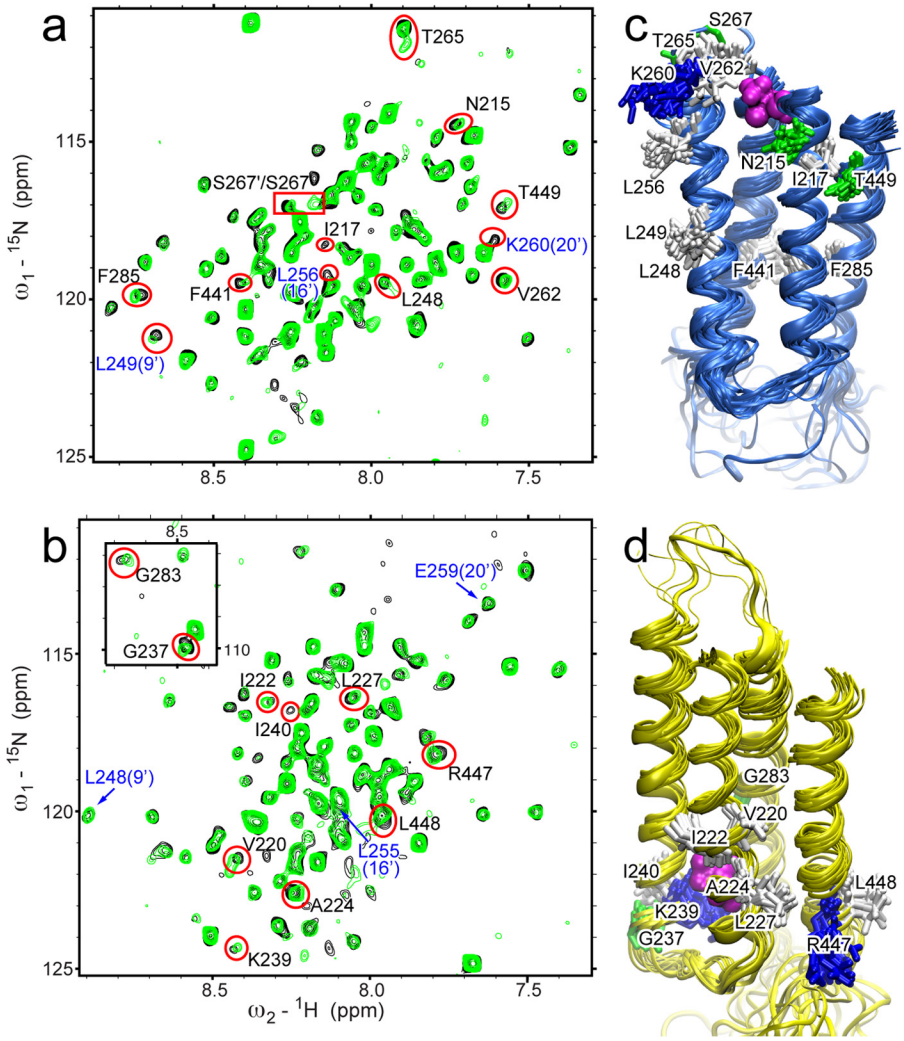

FIGURE 2. **Isoflurane binding to the TM domains of β2 and α7.** *a* and *b*, ^{1}H-^{15}N TROSY-HSQC spectra of β2 (*a*) and α7 (*b*) in the presence (*green*) and absence (*black*) of 1.3 or 1.6 mM isoflurane, respectively. Residues showing significant changes in chemical shift or peak intensity are labeled and highlighted with *red*. Residues labeled in *blue* are pore-lining residues. Full chemical shift assignments for β2 and α7 TM domains are provided in supplemental Figs. S1 and S2, respectively. *c*, the bundle of 20 NMR structures of the β2 TM domain (Protein Data Bank code 2LM2) mapped with residues highlighted in *red* in *a*. *d*, the bundle of 20 NMR structures of the α7 TM domain (Protein Data Bank code 2MAW) mapped with residues highlighted in *red* in *b*. Residues are colored based on residue type: *green*, polar; *white*, nonpolar; and *blue*, basic. Docked isoflurane is shown in *magenta*.

measured isoflurane inhibition by using a repeated application protocol, in which choline was applied at 2-min intervals in the continuous presence of 10 μM isoflurane. Isoflurane progressively inhibited α7β2 currents. Reversibility of isoflurane inhibition was demonstrated by the current recovery after 4 min of isoflurane washout. In contrast to α7β2, the homomeric α7 expressed either in neurons dissociated from VTA (33) or in the SH-EP1 cells (22) are not sensitive to 10 μM isoflurane (Fig. 1, *c* and *d*). This is consistent with an IC_{50} of ~600 μM (~2 minimum alveolar concentration) for the human α7 nAChR reported previously (34). Different sensitivities to isoflurane inhibition were also observed in the recombinant α7β2 and α7 nAChRs expressed in *Xenopus laevis* oocytes. Representative current traces obtained from oocytes (Fig. 1, *e* and *f*) echo the message conveyed by the results from the dissociated neurons (Fig. 1, *a*–*d*). In addition, we found that a swap of residue 22′ between α7 and β2 had a dramatic impact on isoflurane inhibition (Fig. 1, *g* and *h*). Although α7 is insensitive to isoflurane inhibition, the mutant α7-M261(22′)V showed 39 ± 7% ($n = 6$) isoflurane inhibition, similar to that (46 ± 3%, $n = 4$) observed on α7β2. Conversely, the mutant α7β2-V262(22′)M, similar to α7, showed a lower sensitivity to isoflurane inhibition (12 ± 2%, $n = 4$). Altogether, these data suggest an indispensible role for β2 and the importance of its residue Val-262(22′) in isoflurane inhibition.

β2 and α7 Have Different Isoflurane-binding Sites in Their TM Domains—We investigated the binding sites of isoflurane in the TM domains of β2 and α7 nAChRs using high resolution NMR. As shown in the ^{1}H-^{15}N TROSY-HSQC spectra (Fig. 2, *a* and *b*), the presence of 1.3 or 1.6 mM isoflurane perturbed a number of residues in β2 or α7 nAChRs, respectively. The residues with either more than 40% intensity change or a combined chemical shift change (35) greater than 15 ppb (β2) and 10 ppb (α7) were mapped onto NMR structures of the β2 or α7 TM domains (Fig. 2, *c* and *d*). Intrasubunit pockets for isoflurane binding were found in the NMR structures of β2 and α7, but at different sites: the one in α7 is close to the intracellular end of the TM domain, and the one in β2 is at the EC end of the

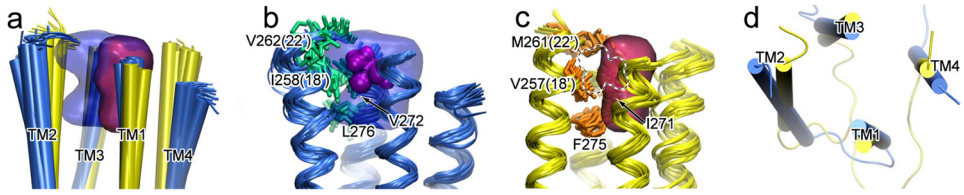

FIGURE 3. **The intrasubunit cavity at the EC end of the TM domain in β2, but not in α7, can accommodate isoflurane binding.** *a*, alignment of 20 NMR structures with the lowest target function for β2 (*blue*) and α7 (*yellow*), and the cavities of β2 (*blue*) and α7 (*red*), outlined by grid points present in at least five of the 20 structures. *b* and *c*, residues highlighted with the side chain bundles (shown in stick representation) in β2 (*b*) and α7 (*c*) have primary responsibility for the different cavity volumes. Note that in β2, the cavity can accommodate isoflurane (*purple* surface), but the cavity in α7 (*dotted outline*) cannot do the same. *d*, the top view of the lowest target function structures of β2 (*blue*) and α7 (*yellow*) shows different orientations of TM helices.

TM domain, which is also the site for halothane and ketamine binding (36). Moreover, this anesthetic site in β2 is homologous to the previously identified anesthetic site in GLIC (37), ELIC (18), and the *Torpedo* nAChR (38). The isoflurane site in α7 is homologous to a halothane binding site at the IC end of the β2 TM domain identified by NMR and coincides with one of the halothane sites in α7 predicted by our previous molecular dynamics simulations (19).

Some residues, including the channel gate residue Leu-249(9′) in β2, showed significant changes upon the addition of isoflurane but are structurally remote from the cluster of residues defining the binding pocket. Their changes likely result from allosteric effects rather than direct contact with isoflurane. It is also worth noting that several pore-lining residues in β2, but not α7, showed greatly reduced intensity upon the addition of isoflurane, indicative of motional changes for these residues.

A Smaller Intrasubunit Pocket Excludes Isoflurane Binding to the EC end of the α7 TM Domain—To determine why isoflurane binds to the EC end of the TM domain in β2 but not in α7, we examined the pocket in this region based on NMR structures of the β2 and α7 TM domains. Mostly hydrophobic residues and a few hydrophilic residues from four TM helices line the intrasubunit pocket near the EC end of the TM helices in both β2 and α7. The average cavity volumes are 179 ± 12 and 122 ± 10 Å^3 for β2 and α7, respectively (Fig. 3). The differences in cavity volume primarily result from tighter packing of four helices in the region of α7 and greater side chain volume of several cavity-lining residues in α7, such as α7-M261(22′) *versus* β2-V262(22′), α7-I271 *versus* β2-V272, and α7-F275 *versus* β2-L276. The differences in isoflurane inhibition made by these residues were evident in functional measurements of the mutants α7-M261(22′)V and α7β2-V262(22′)M (Fig. 1, *g* and *h*). Helical tilting differences (6.7 ± 1.3°), measured by angles between TM2 and TM4 (Fig. 3*d*), also contribute to different cavity volumes at the EC end of the TM domain between β2 and α7. Both the inward helical tilting of α7 and the more bulky M22′ side chain in α7 contribute to a smaller cavity. Furthermore, orientations of side chains also affect the cavity volumes. For the residues in TM3, both side chains of β2-V272 and β2-L276 are oriented away from the cavity, whereas the equivalent residues α7-I271 and α7-F275 are oriented toward the cavity. A smaller cavity in the EC end of the TM domain in α7 has reduced the probability of isoflurane binding to the region, considering that isoflurane has a volume of 144 Å^3 (39).

Isoflurane Modulates the Dynamics of α7 and β2 Differently—One of the most striking differences between α7 and β2 is that upon isoflurane binding, α7 retained a single signal for each residue in the NMR spectra, but β2 showed classic examples of two-site chemical exchange (40, 41) for several residues, including the channel gate residue Leu-249(9′) and Val-262(22′) lining the isoflurane-binding pocket in β2. As shown in Fig. 4, in the absence of isoflurane (*black*), each of these β2 residues showed a single peak in the NMR spectrum. After adding 1.3 mM isoflurane (*red*), an additional peak became observable for Leu-248 and Thr-265 (denoted as Leu-248′ and Thr-265′, respectively). When the isoflurane concentration was increased to 3 mM (*cyan*), Leu-249 and Val-262 also showed additional peaks. The combined chemical shift change between each pair of peaks (A-B or A′-B), $\Delta\omega_{H+N} = [(\Delta\omega_H{}^2 + \Delta\omega_N{}^2)]^{1/2}$ is 32, 27, 37, 32 Hz for Leu-248, Leu-249, Val-262, and Thr-265 of β2, respectively. Based on the consensus from many previous studies (40–42), the occurrence of two distinct peaks for a residue indicates a slow exchange with $k_{ex} \ll 2\pi\Delta\omega_{H+N} \sim 200\ s^{-1}$.

Conformational exchange among β2 residues also shows some differences. For residues Leu-248 and Thr-265, peak A remained at 20-Hz line width and the same resonance frequency in the absence and presence of isoflurane, indicating a possibility that slow conformational exchange with an extremely low population for the second conformation (peak B) already existed in the absence of isoflurane. Isoflurane shifted the equilibria between the two conformations. Indeed, the population of conformation B, $p_B = 1 - p_A$, increased from 0 to ~0.3 and more than ~0.5 when isoflurane was increased from 0 to 1.3 and 3 mM. Overall, Leu-248 and Thr-265 fit well to the scheme of slow exchange between two conformations (40–42). In the case of Leu-249 and Val-262, however, a single peak with a broader line width in the ^{1}H dimension was observed in the presence of 0 mM (Leu-249, 21 Hz; Val-262, 17 Hz) and 1.3 mM isoflurane (Leu-249, 19 Hz; Val-262, 16 Hz), but two narrower peaks (Leu-249, 16 and 12 Hz; Val-262, 14 and 12 Hz) were observed in the presence of 3 mM isoflurane. The results suggest that Leu-249 and Val-262 were likely in an intermediate exchange regime (40, 41) before being exposed to 3 mM isoflurane. In addition to slower exchange between A′ and B conformations, the increased isoflurane concentration also shifted peak A′ from peak A by 14 and 11 Hz for Leu-249 and Val-262, respectively (Fig. 4). This is not unexpected, considering that multiple conformers with subtle differences can coexist in a functional state (43, 44). The sensitivity of β2 and insensitivity of α7 to the dynamics modulation by isoflurane are in good agreement with their distinctly different functional responses to isoflurane inhibition.

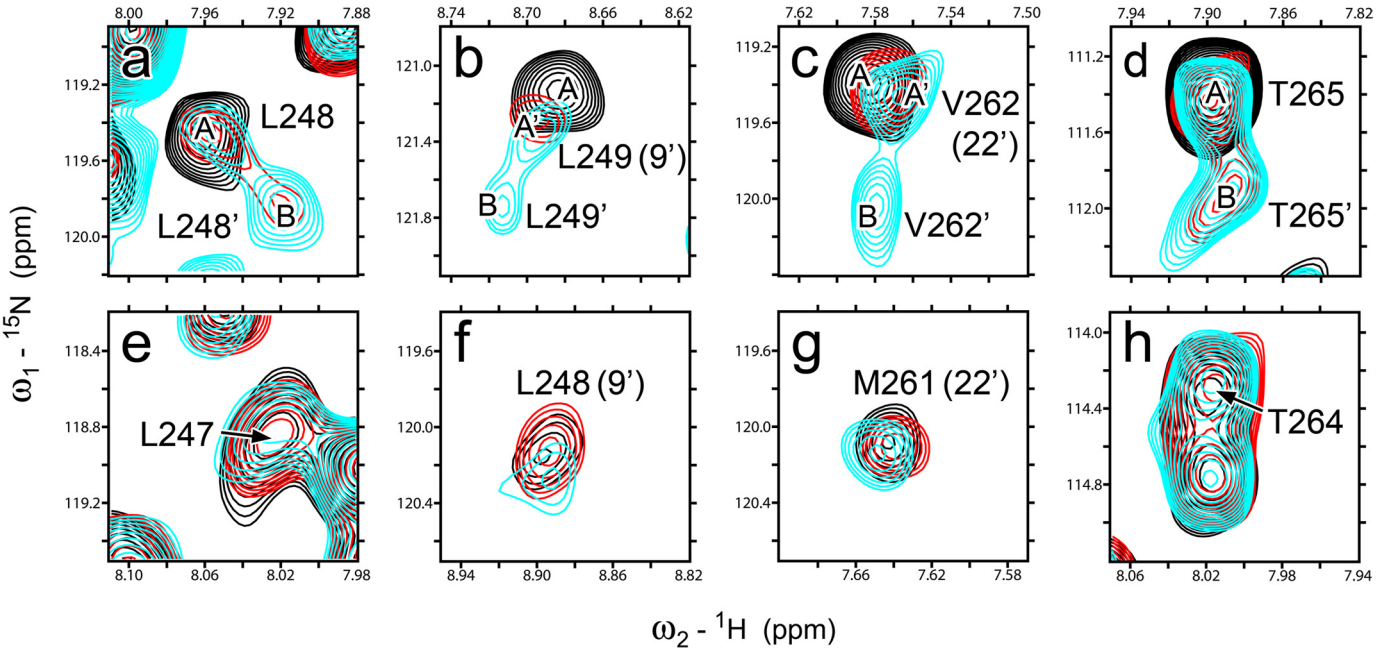

FIGURE 4. **Different dynamics responses of β2 and α7 to isoflurane modulation.** Overlay of NMR spectra for individual residues in β2 (*a–d*) and α7 (*e–h*) in the presence of isoflurane: 0 mM (*black*), 1.3 mM for β2 and 1.6 mM for α7 (*red*), and 3.0 mM for β2 and 3.3 mM for α7 (*cyan*). Note that none of the α7 residues show an additional conformation over the isoflurane concentration range used in the experiments. The peaks representing the different conformations for β2 are labeled *A*, *A′*, and *B*.

DISCUSSION

Our functional data substantiate the previous prediction (19) that, unlike the α7 nAChR, the α7β2 nAChR is sensitive to anesthetic inhibition. The result highlights the role of β2 in functional modulation by volatile anesthetics and supports our hypothesis that β2 is primarily responsible for the difference of anesthetic susceptibility between α4β2 and α7 (19). More importantly, the result conveys the message that two or three subunits susceptible to anesthetics, such as β2 in α7β2, are sufficient to produce functional effects. The message is consistent with the notion obtained from molecular dynamics simulations of anesthetic propofol action in GLIC (45).

Why is β2 more susceptible to volatile anesthetics than α7? This key question has been addressed by our NMR experiments from three aspects. First, β2 and α7 show some structural differences in their TM domains, even though they share a common scaffold. The most notable difference lies in the size of an intrasubunit cavity near the EC end of the TM domain that is large enough in β2, but not in α7, to accommodate isoflurane binding. Second, the structural difference leads to different binding locations for isoflurane, which binds to the cavity at the EC end of the TM domain in β2 but to a pocket located at the IC end of the TM domain in α7. Finally, differences in their structures and isoflurane-binding sites may have contributed to different dynamics responses of β2 and α7 to isoflurane binding. Only in β2 were isoflurane-induced changes in conformational populations and motion on the μs-ms time scale observed. The combined effects from structures, anesthetic binding sites, and dynamics modulations may have contributed to the functional differences between β2 and α7.

The sequence identity between β2 and α7 is high, ~50% for the TM domain and close to 65% for the pore-lining TM2 helix. Their sequence homology is even higher (Fig. 5). Our results

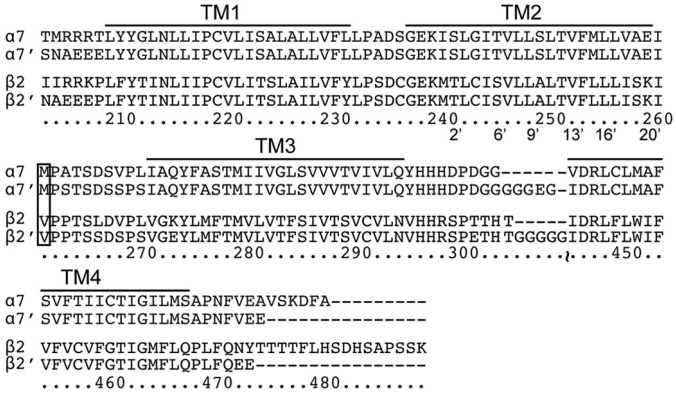

FIGURE 5. **Sequence alignments for TM domains of human α7 and β2 nAChRs.** Sequences of the constructs used for NMR samples, α7′ and β2′, are aligned with their respective native sequences. Note that only a few terminal and loop residues were changed to increase the stability of NMR samples. The labeled sequence numbers are for the α7 nAChR. The pore lining residues are labeled using the conventional prime numbering. Residues in the *box* were mutated in the study.

demonstrate that variation in a small number of residues is sufficient to make differences in protein structures, drug-binding sites, and functional responses to drug binding. The functional significance of such small changes in structure highlights the necessity of solving individual protein structures, even for highly homologous proteins. In the case of β2 and α7, the homologous cavity-lining residues β2-V22′ and α7-M22′ make a notable difference for their respective cavities, isoflurane binding, and isoflurane inhibition. Indeed, a single α7-M22′V mutation markedly increased the channel sensitivity to isoflurane, and the α7β2-V22′M mutation had a reverse effect. This result is consistent with the diminished sensitivity to volatile anesthetics observed previously for the I22′M mutation in the α3 containing nAChR (46). A larger volume and extended side

chain conformation of Met-22′ can effectively reduce the cavity volume and obstruct drug binding. Moreover, methionine may also stabilize the TM2 helix and make it more resilient to structural and dynamic perturbation introduced by anesthetic binding. Previous studies using unnatural amino acid substitutions have shown that residues with unbranched side chains, such as methionine and alanine, have a more stabilizing effect on α helices than branched amino acids, such as valine and isoleucine (47). Similarly, β2-S19′ and α7-A19′ could also make dynamics differences to the TM2 helix. Alanine is a natural helix promoter (48), whereas serine and threonine often disrupt α-helices because of backbone to side chain hydrogen bonds (49, 50). Our previous NMR study noted heightened conformational dynamics at the EC end of TM2 for the glycine receptor, which is uniquely rich with serines in this region compared with other pLGICs (51). Contributions to the anesthetic binding site from two pairs of residues in TM3, β2-L276/α7-F275 and β2-V272/α7-I271, should also not be underestimated. Mutation on the homologous residue in GLIC was found to significantly affect the susceptibility of the channel to the anesthetics desflurane and propofol (37).

The anesthetic binding site at the EC end of the TM domain, as revealed for isoflurane in β2, is probably a common site in pLGICs for anesthetics. Using NMR, we found that the anesthetics halothane and ketamine bound to the same site in β2 (36). The site is also consistent with one of the halothane sites identified by photo affinity labeling in the *Torpedo* nAChR (38) and by fluorescence quenching in GLIC (52). The anesthetics desflurane and propofol were found in the homologous site in the crystal structures of GLIC bound with these anestethics (37). Functional and mutation studies on the α7/α3 nAChR chimeras also underscored the importance of the cavity to inhibition by the volatile anesthetic halothane (46). In contrast, anesthetic binding to the IC end of the TM domain, as observed for isoflurane in α7 in this study, is less effective to perturb channel function. Isoflurane inhibits α7 only at concentrations higher than those used clinically (34).

Our results provide evidence that functional insensitivity of α7 to volatile anesthetics is not due to a lack of anesthetic binding, at least in the case of isoflurane. The hypersensitivity of α7β2 and the insensitivity of α7 suggest that the EC end of the TM domain plays a critical role for channel gating in pLGICs. Increasing the rigidity of residues at the EC end of the TM domain can make the channel less responsive to activation signals. Many previous studies support this notion. Increasing helical flexibility at the EC end of TM2 of the nAChR was found to increase the sensitivity of the receptors to agonist more than 10-fold (53). Disulfide bond trapping experiments on the $GABA_A$ receptor (54) and EPR experiments on GLIC (55) also support heightened dynamics at the EC end of TM2 during channel gating. Our previous work on the glycine receptor suggested that increasing or decreasing the conformational dynamics at the EC end of TM2 could respectively increase or decrease the susceptibility of the channel to allosteric modulation (51). Thus, it is conceivable that changing dynamics of the EC end of the TM domain, either via drug binding or via point mutations, is a common mechanism to modulate the functions of pLGICs.

Our study not only highlights the importance of the anesthetic binding site but also emphasizes the role of channel dynamics in anesthetic action. Although β2 and α7 have high sequence homology, the dynamics and subtle structural differences are sufficient to affect anesthetic binding as well as functional consequences. Anesthetic binding is necessary but not sufficient to produce a functional consequence. Only the binding that modulates dynamics of pore-lining residues, such as that at the EC end of the β2 TM domain, can impact function.

Acknowledgments—The plasmids encoding human α7 and β2 nAChRs for oocyte expression were gifts from Prof. Lindstrom's lab at the University of Pennsylvania and Prof. Henry Lester's lab at the California Institute of Technology, respectively.

REFERENCES

1. Palma, E., Maggi, L., Barabino, B., Eusebi, F., and Ballivet, M. (1999) Nicotinic acetylcholine receptors assembled from the α7 and β3 subunits. *J. Biol. Chem.* **274,** 18335–18340
2. Khiroug, S. S., Harkness, P. C., Lamb, P. W., Sudweeks, S. N., Khiroug, L., Millar, N. S., and Yakel, J. L. (2002) Rat nicotinic ACh receptor α7 and β2 subunits co-assemble to form functional heteromeric nicotinic receptor channels. *J. Physiol.* **540,** 425–434
3. Liu, Q., Huang, Y., Xue, F., Simard, A., DeChon, J., Li, G., Zhang, J., Lucero, L., Wang, M., Sierks, M., Hu, G., Chang, Y., Lukas, R. J., and Wu, J. (2009) A novel nicotinic acetylcholine receptor subtype in basal forebrain cholinergic neurons with high sensitivity to amyloid peptides. *J. Neurosci.* **29,** 918–929
4. Picciotto, M. R., Zoli, M., Léna, C., Bessis, A., Lallemand, Y., Le Novère, N., Vincent, P., Pich, E. M., Brûlet, P., and Changeux, J. P. (1995) Abnormal avoidance learning in mice lacking functional high-affinity nicotine receptor in the brain. *Nature* **374,** 65–67
5. Marubio, L. M., del Mar Arroyo-Jimenez, M., Cordero-Erausquin, M., Léna, C., Le Novère, N., de Kerchove d'Exaerde, A., Huchet, M., Damaj, M. I., and Changeux, J. P. (1999) Reduced antinociception in mice lacking neuronal nicotinic receptor subunits. *Nature* **398,** 805–810
6. Xu, W., Orr-Urtreger, A., Nigro, F., Gelber, S., Sutcliffe, C. B., Armstrong, D., Patrick, J. W., Role, L. W., Beaudet, A. L., and De Biasi, M. (1999) Multiorgan autonomic dysfunction in mice lacking the β2 and the β4 subunits of neuronal nicotinic acetylcholine receptors. *J. Neurosci.* **19,** 9298–9305
7. Violet, J. M., Downie, D. L., Nakisa, R. C., Lieb, W. R., and Franks, N. P. (1997) Differential sensitivities of mammalian neuronal and muscle nicotinic acetylcholine receptors to general anesthetics. *Anesthesiology* **86,** 866–874
8. Mori, T., Zhao, X., Zuo, Y., Aistrup, G. L., Nishikawa, K., Marszalec, W., Yeh, J. Z., and Narahashi, T. (2001) Modulation of neuronal nicotinic acetylcholine receptors by halothane in rat cortical neurons. *Mol. Pharmacol.* **59,** 732–743
9. Flood, P., Ramirez-Latorre, J., and Role, L. (1997) α4β2 neuronal nicotinic acetylcholine receptors in the central nervous system are inhibited by isoflurane and propofol, but α7-type nicotinic acetylcholine receptors are unaffected. *Anesthesiology* **86,** 859–865
10. Bondarenko, V., Mowrey, D., Tillman, T., Cui, T., Liu, L. T., Xu, Y., and Tang, P. (2012) NMR structures of the transmembrane domains of the α4β2 nAChR. *Biochim. Biophys. Acta* **1818,** 1261–1268
11. Unwin, N. (2005) Refined structure of the nicotinic acetylcholine receptor at 4A resolution. *J. Mol. Biol.* **346,** 967–989
12. Bocquet, N., Nury, H., Baaden, M., Le Poupon, C., Changeux, J. P., Delarue, M., and Corringer, P. J. (2009) X-ray structure of a pentameric ligand-gated ion channel in an apparently open conformation. *Nature* **457,** 111–114
13. Hilf, R. J., and Dutzler, R. (2009) Structure of a potentially open state of a proton-activated pentameric ligand-gated ion channel. *Nature* **457,** 115–118

14. Pan, J., Chen, Q., Willenbring, D., Mowrey, D., Kong, X.-P., Cohen, A., Divito, C. B., Xu, Y., and Tang, P. (2012) Structure of the pentameric ligand-gated ion channel GLIC bound with anesthetic ketamine. *Structure* **20,** 1463–1469
15. Sauguet, L., Poitevin, F., Murail, S., Van Renterghem, C., Moraga-Cid, G., Malherbe, L., Thompson, A. W., Koehl, P., Corringer, P. J., Baaden, M., and Delarue, M. (2013) Structural basis for ion permeation mechanism in pentameric ligand-gated ion channels. *EMBO J.* **32,** 728–741
16. Hilf, R. J., and Dutzler, R. (2008) X-ray structure of a prokaryotic pentameric ligand-gated ion channel. *Nature* **452,** 375–379
17. Pan, J., Chen, Q., Willenbring, D., Yoshida, K., Tillman, T., Kashlan, O. B., Cohen, A., Kong, X. P., Xu, Y., and Tang, P. (2012) Structure of the pentameric ligand-gated ion channel ELIC cocrystallized with its competitive antagonist acetylcholine. *Nat. Commun.* **3,** 714
18. Spurny, R., Billen, B., Howard, R. J., Brams, M., Debaveye, S., Price, K. L., Weston, D. A., Strelkov, S. V., Tytgat, J., Bertrand, S., Bertrand, D., Lummis, S. C., and Ulens, C. (2013) Multisite binding of a general anesthetic to the prokaryotic pentameric *Erwinia chrysanthemi* ligand-gated ion channel (ELIC). *J. Biol. Chem.* **288,** 8355–8364
19. Mowrey, D., Haddadian, E. J., Liu, L. T., Willenbring, D., Xu, Y., and Tang, P. (2010) Unresponsive correlated motion in α7 nAChR to halothane binding explains its functional insensitivity to volatile anesthetics. *J. Phys. Chem. B* **114,** 7649–7655
20. Liu, L. T., Willenbring, D., Xu, Y., and Tang, P. (2009) General anesthetic binding to neuronal $\alpha4\beta2$ nicotinic acetylcholine receptor and its effects on global dynamics. *J. Phys. Chem. B* **113,** 12581–12589
21. Liu, L. T., Haddadian, E. J., Willenbring, D., Xu, Y., and Tang, P. (2010) Higher susceptibility to halothane modulation in open- than in closed-channel $\alpha4\beta2$ nAChR revealed by molecular dynamics simulations. *J. Phys. Chem. B* **114,** 626–632
22. Zhao, L., Kuo, Y. P., George, A. A., Peng, J. H., Purandare, M. S., Schroeder, K. M., Lukas, R. J., and Wu, J. (2003) Functional properties of homomeric, human α7-nicotinic acetylcholine receptors heterologously expressed in the SH-EP1 human epithelial cell line. *J. Pharmacol. Exp. Ther.* **305,** 1132–1141
23. Dascal, N. (2001) Voltage clamp recordings from *Xenopus* oocytes. *Current Protocols in Neuroscience* (Crawley, J. N., McKay, Ra., and Rogawski, M. A., eds) Chapter 6, Unit 6.12, John Wiley and Sons, Hoboken, NJ.
24. Xu, Y., Seto, T., Tang, P., and Firestone, L. (2000) NMR study of volatile anesthetic binding to nicotinic acetylcholine receptors. *Biophys. J.* **78,** 746–751
25. Wishart, D. S., Bigam, C. G., Yao, J., Abildgaard, F., Dyson, H. J., Oldfield, E., Markley, J. L., and Sykes, B. D. (1995) ^{1}H, ^{13}C and ^{15}N chemical shift referencing in biomolecular NMR. *J. Biomol. NMR* **6,** 135–140
26. Delaglio, F., Grzesiek, S., Vuister, G. W., Zhu, G., Pfeifer, J., and Bax, A. (1995) NMRPipe. A multidimensional spectral processing system based on UNIX pipes. *J. Biomol. NMR* **6,** 277–293
27. Goddard, T. D., and Kneller, D. G. (2001) *SPARKY 3,* University of California, San Francisco
28. Morris, G. M., Goodsell, D. S., Halliday, R. S., Huey, R., Hart, W. E., Belew, R. K., and Olson, A. J. (1998) Automated docking using a Lamarckian genetic algorithm and an empirical binding free energy function. *J. Comput. Chem.* **19,** 1639–1662
29. Durrant, J. D., de Oliveira, C. A., and McCammon, J. A. (2011) POVME. An algorithm for measuring binding-pocket volumes. *J. Mol. Graph. Model* **29,** 773–776
30. Humphrey, W., Dalke, A., and Schulten, K. (1996) VMD. Visual molecular dynamics. *J. Mol. Graph.* **14,** 33–38
31. Yamashita, M., Mori, T., Nagata, K., Yeh, J. Z., and Narahashi, T. (2005) Isoflurane modulation of neuronal nicotinic acetylcholine receptors expressed in human embryonic kidney cells. *Anesthesiology* **102,** 76–84
32. Nickalls, R. W., and Mapleson, W. W. (2003) Age-related iso-MAC charts for isoflurane, sevoflurane and desflurane in man. *Br. J. Anaesth.* **91,** 170–174
33. Wu, J., George, A. A., Schroeder, K. M., Xu, L., Marxer-Miller, S., Lucero, L., and Lukas, R. J. (2004) Electrophysiological, pharmacological, and molecular evidence for α7-nicotinic acetylcholine receptors in rat midbrain dopamine neurons. *J. Pharmacol. Exp. Ther.* **311,** 80–91
34. Flood, P., and Coates, K. M. (2002) Sensitivity of the α7 nicotinic acetylcholine receptor to isoflurane may depend on receptor inactivation. *Anesth. Analg.* **95,** 83–87
35. Schumann, F. H., Riepl, H., Maurer, T., Gronwald, W., Neidig, K. P., and Kalbitzer, H. R. (2007) Combined chemical shift changes and amino acid specific chemical shift mapping of protein-protein interactions. *J. Biomol. NMR* **39,** 275–289
36. Bondarenko, V., Mowrey, D., Liu, L. T., Xu, Y., and Tang, P. (2013) NMR resolved multiple anesthetic binding sites in the TM domains of the $\alpha4\beta2$ nAChR. *Biochim. Biophys. Acta* **1828,** 398–404
37. Nury, H., Van Renterghem, C., Weng, Y., Tran, A., Baaden, M., Dufresne, V., Changeux, J. P., Sonner, J. M., Delarue, M., and Corringer, P. J. (2011) X-ray structures of general anaesthetics bound to a pentameric ligand-gated ion channel. *Nature* **469,** 428–431
38. Chiara, D. C., Dangott, L. J., Eckenhoff, R. G., and Cohen, J. B. (2003) Identification of nicotinic acetylcholine receptor amino acids photolabeled by the volatile anesthetic halothane. *Biochemistry* **42,** 13457–13467
39. Jenkins, A., Greenblatt, E. P., Faulkner, H. J., Bertaccini, E., Light, A., Lin, A., Andreasen, A., Viner, A., Trudell, J. R., and Harrison, N. L. (2001) Evidence for a common binding cavity for three general anesthetics within the GABAA receptor. *J. Neurosci.* **21,** RC136
40. Mittermaier, A. K., and Kay, L. E. (2009) Observing biological dynamics at atomic resolution using NMR. *Trends Biochem. Sci.* **34,** 601–611
41. Kleckner, I. R., and Foster, M. P. (2011) An introduction to NMR-based approaches for measuring protein dynamics. *Biochim. Biophys. Acta* **1814,** 942–968
42. Palmer, A. G., 3rd, Kroenke, C. D., and Loria, J. P. (2001) Nuclear magnetic resonance methods for quantifying microsecond-to-millisecond motions in biological macromolecules. *Methods Enzymol.* **339,** 204–238
43. Prevost, M. S., Sauguet, L., Nury, H., Van Renterghem, C., Huon, C., Poitevin, F., Baaden, M., Delarue, M., and Corringer, P. J. (2012) A locally closed conformation of a bacterial pentameric proton-gated ion channel. *Nat. Struct. Mol. Biol.* **19,** 642–649
44. Yamodo, I. H., Chiara, D. C., Cohen, J. B., and Miller, K. W. (2010) Conformational changes in the nicotinic acetylcholine receptor during gating and desensitization. *Biochemistry* **49,** 156–165
45. Mowrey, D., Cheng, M. H., Liu, L. T., Willenbring, D., Lu, X., Wymore, T., Xu, Y., and Tang, P. (2013) Asymmetric Ligand Binding Facilitates Conformational Transitions in Pentameric Ligand-Gated Ion Channels. *J. Am. Chem. Soc.* **135,** 2172–2180
46. Downie, D. L., Vicente-Agullo, F., Campos-Caro, A., Bushell, T. J., Lieb, W. R., and Franks, N. P. (2002) Determinants of the anesthetic sensitivity of neuronal nicotinic acetylcholine receptors. *J. Biol. Chem.* **277,** 10367–10373
47. Lyu, P. C., Sherman, J. C., Chen, A., and Kallenbach, N. R. (1991) α-helix stabilization by natural and unnatural amino acids with alkyl side chains. *Proc. Natl. Acad. Sci. U.S.A.* **88,** 5317–5320
48. Richardson, J. S., and Richardson, D. C. (1988) Amino acid preferences for specific locations at the ends of α helices. *Science* **240,** 1648–1652
49. Ballesteros, J. A., Deupi, X., Olivella, M., Haaksma, E. E., and Pardo, L. (2000) Serine and threonine residues bend α-helices in the $\chi_1 = g(-)$ conformation. *Biophys. J.* **79,** 2754–2760
50. Varga, Z., and Kovacs, A. (2005) Hydrogen bonding in peptide secondary structures. *Int. J. Quant. Chem.* **105,** 302–312
51. Mowrey, D. D., Cui, T., Jia, Y., Ma, D., Makhov, A. M., Zhang, P., Tang, P., and Xu, Y. (2013) Open-channel structures of the human glycine receptor α1 full-length transmembrane domain. *Structure* **21,** 1897–1904
52. Chen, Q., Cheng, M. H., Xu, Y., and Tang, P. (2010) Anesthetic binding in a pentameric ligand-gated ion channel. GLIC. *Biophys. J.* **99,** 1801–1809
53. England, P. M., Zhang, Y., Dougherty, D. A., and Lester, H. A. (1999) Backbone mutations in transmembrane domains of a ligand-gated ion channel. Implications for the mechanism of gating. *Cell* **96,** 89–98
54. Horenstein, J., Wagner, D. A., Czajkowski, C., and Akabas, M. H. (2001) Protein mobility and GABA-induced conformational changes in $GABA_A$ receptor pore-lining M2 segment. *Nat. Neurosci.* **4,** 477–485
55. Velisetty, P., Chalamalasetti, S. V., and Chakrapani, S. (2012) Conformational transitions underlying pore opening and desensitization in membrane-embedded *Gloeobacter violaceus* ligand-gated ion channel (GLIC). *J. Biol. Chem.* **287,** 36864–36872